Chem

CellPress

Article

Toward Design Rules for Enzyme Immobilization in Hierarchical Mesoporous Metal-Organic Frameworks

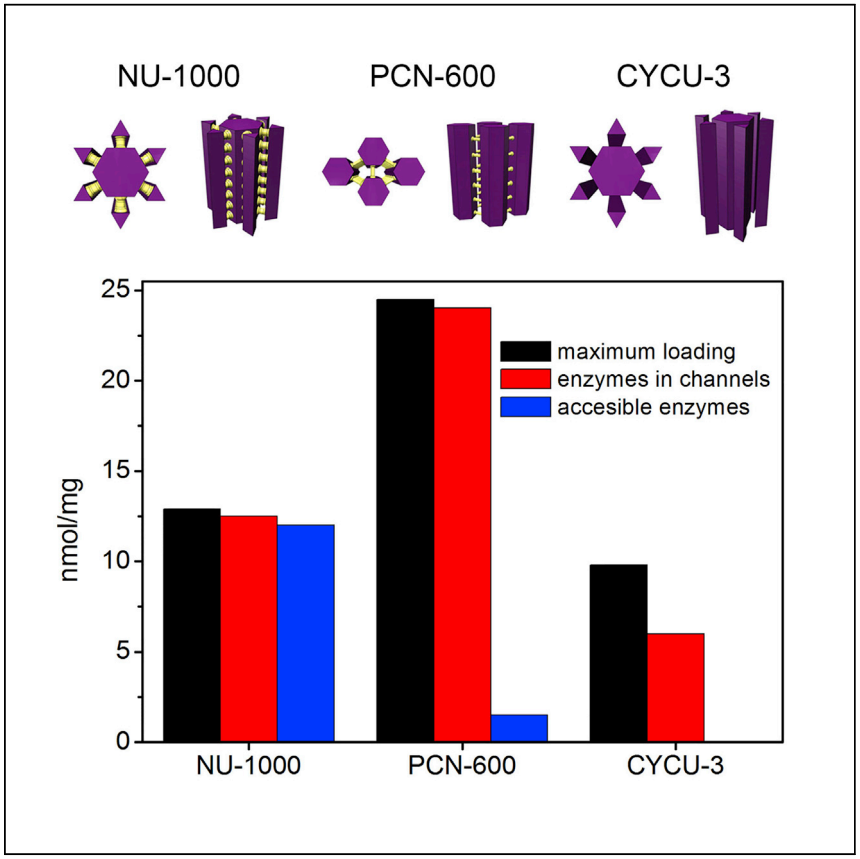

Metal-organic frameworks (MOFs) are porous, crystalline materials comprised of metal nodes and organic linkers. Here, a Zr-based MOF named NU-1000 is used to encapsulate and protect an enzyme. The encapsulation and subsequent protection of enzymes in solid supports is important for the potential industrialization of enzymes as chemical catalysts. NU-1000 is shown to be capable of stabilizing the enzyme under harsh conditions, and in addition, the encapsulated enzyme is shown to maintain full functionality.

Peng Li, Justin A. Modica, Ashlee J. Howarth, ..., Milan Mrksich, Joseph T. Hupp, Omar K. Farha

o-farha@northwestern.edu

HIGHLIGHTS

Enzyme immobilization in a metal-organic framework with a hierarchical pore structure

Excellent enzyme accessibility and activity after encapsulation

Improved enzyme stability under harsh conditions after encapsulation

Li et al., Chem 1, 154–169
July 7, 2016
http://dx.doi.org/10.1016/j.chempr.2016.05.001

Chem

CellPress

Article

Toward Design Rules for Enzyme Immobilization in Hierarchical Mesoporous Metal-Organic Frameworks

Peng Li,[1,5] Justin A. Modica,[2,5] Ashlee J. Howarth,[1] Ernesto Vargas L.,[3] Peyman Z. Moghadam,[3] Randall Q. Snurr,[3] Milan Mrksich,[1,2] Joseph T. Hupp,[1] and Omar K. Farha[1,4,6,*]

SUMMARY

The immobilization of enzymes on or in solid supports is crucial for the industrialization of enzymes as chemical catalysts because immobilization provides stabilization, easy separation, and recyclability. Here, we show that a water-stable metal-organic framework, NU-1000, with hierarchical pore structure has the right combination of properties to be particularly well-suited as a scaffold for immobilizing enzymes such that they maintain full enzymatic catalytic activity. The immobilized enzyme shows greater resistance to organic solvent and denaturant than does the free enzyme and is characterized by greater reactant accessibility and higher activity than the same enzyme encapsulated in topologically simpler metal-organic frameworks. These findings suggest design rules for hierarchical pore structuring of host frameworks for enzyme-encapsulation applications by demonstrating enzyme immobilization in a solid support whereby the enzyme is highly accessible and retains catalytic activity under chemically challenging conditions.

INTRODUCTION

Enzyme-mediated catalysis is a practical, sustainable, and environmentally benign strategy for the production of industrially relevant chemicals ranging from biofuels to pharmaceuticals and food additives.[1] Advances in protein engineering have led to enzymes with enhanced catalytic performance, yet their use industrially is often hampered by the lack of long-term stability, recyclability, and efficient recovery.[2] These issues can be overcome by using a solid support to immobilize the enzymes and shield them from deactivating reaction conditions (e.g., organic solvents[3] and denaturants[4]) in addition to providing potential for enzyme recyclability via recovery of the heterogenized catalyst and support.

Metal-organic frameworks (MOFs) are promising candidates for enzyme immobilization.[5–11] MOFs[12] are a class of highly tunable, porous materials that have shown promise in a wide range of potential applications including gas storage and release,[13–15] light harvesting and energy conversion,[16–18] drug delivery,[19] and catalysis.[20] MOFs are potentially superior to other porous materials commonly used to immobilize proteins and enzymes such as sol gels,[21] zeolites,[22] and mesoporous silica supports,[23–25] because MOFs are finely tunable and crystalline, thus exhibiting uniformity and long-range ordering from the atomic to microscale regime.[12] Enzyme immobilization in less uniform solid supports typically leads to low protein-loading efficiency,[22,26] low stability at elevated temperatures, and/or enzyme leaching.[27,28] Initial studies have shown that some of these challenges can be overcome by using

The Bigger Picture

Metal-organic frameworks (MOFs), which are simplistically viewed as molecular sponges, have garnered widespread media attention in recent years because of their potential in many popular applications, including natural-gas-powered vehicles. MOFs are porous yet robust materials that offer an interesting platform for encapsulating and protecting enzymes from degradation. Enzymes are nature's catalysts, and the delicate structure of enzymes can be understood by considering the irreversibility of frying an egg. In order to apply enzymes broadly as catalysts in industry, the need to protect them from denaturation under harsh conditions is important. Here, we show the applicability of a robust MOF that has structural features that make it intriguing for enzyme encapsulation. The results are important because the enzyme is protected and maintains high enzymatic activity. The long-term goal is to encapsulate specific enzymes that can be used for the detoxification of chemical-warfare agents.

MOFs for enzyme immobilization.[5–11] These initial studies focused on placing enzymes in cage-like materials without emphasis on the spatial distribution, accessibility, or conformation of the encapsulated enzyme or the diffusion of reactants and products throughout a given support. These characteristics coupled with composite stability, however, are critical design elements of an optimal MOF bioreactor.[21]

We reasoned that an ideal enzyme support should present a hierarchical pore structure with large pores for enzyme immobilization and small pores for reactant/product diffusion. We have recently described the preparation and characterization of the water-stable, mesoporous, zirconium-based MOF NU-1000,[29] which features hexagonal channels with a diameter of 3.1 nm as well as triangular channels with an edge length of 1.5 nm and windows connecting the two channels (Figure 1). We reasoned that an MOF with this unusual hierarchical pore structure would be especially suitable for the encapsulation of *Fusarium solani pisi* cutinase (PDB: 1CEX), an esterase that has shown promise as a biocatalyst in the preparation of aliphatic esters.[30–33] The sizes of the larger channels of NU-1000 match that of cutinase, an ellipsoid-shaped protein featuring a small-axis length of ~3.0 nm.[34] These features, in addition to the high chemical (at pH 1–11)[35] and thermal stability (at >450°C)[29] of NU-1000, make this MOF a promising candidate material for use as a solid support in biocatalysis.

RESULTS AND DISCUSSION

Cutinase Immobilization

We treated 5-μm-long activated crystals of the MOF (NU-1000-5 μm) with a Tris-buffered saline (TBS) solution of cutinase (100 μM, pH 7.4) at 25°C (Figure 1). The uptake of cutinase by NU-1000-5 μm was determined using UV-visible spectroscopy, and a maximum loading of 5 μmol/g was reached after ~75 hr (Figure S1). The solid sample (hereafter denoted as cutinase@NU-1000-5 μm) was then washed five times with detergent-containing buffer solution to ensure full removal of any loosely bound cutinase. Inductively coupled plasma-optical emission spectroscopy (ICP-OES) of the washed cutinase@NU-1000-5 μm sample also revealed a cutinase uptake of 5 μmol/g. The powder X-ray diffraction (PXRD) pattern of NU-1000-5 μm before and after cutinase immobilization confirmed that bulk crystallinity was retained after cutinase encapsulation (Figure 2A). Cutinase@NU-1000-5 μm exhibited a type IV N_2 adsorption-desorption isotherm, much like NU-1000-5 μm itself, but not surprisingly, the MOF exhibited a lower N_2 uptake capacity when cutinase was present in the pores (Figure 2B). The density functional theory pore-size distribution analysis of activated NU-1000-5 μm and cutinase@NU-1000-5 μm showed the two different pores in the hierarchical structure (Figure 2C). The pore volume corresponding to the triangular channels of NU-1000-5 μm dropped from 0.50 to 0.44 cm^3/g, whereas the pore volume corresponding to the hexagonal channels dropped from 0.75 to 0.22 cm^3/g after cutinase encapsulation.

To confirm that cutinase was internalized within NU-1000 and not simply adsorbed on the external surface or within defects of the crystal, we used in situ confocal laser scanning microscopy (CLSM) to image the cutinase encapsulation process with an AlexaFluor 647-labeled enzyme (Cut647) (Figure S1). To study the effect of crystal length on enzyme diffusion, we synthesized NU-1000 crystals with an average length of 10 and 1.5 μm (Figures 3A and 3B). The crystals were immersed in a 50 μM solution of Cut647, and 2D (xy) fluorescence intensity profiles of the MOF samples were obtained at a fixed z depth corresponding to the center layer of the crystal. These

[1]Department of Chemistry, International Institute for Nanotechnology

[2]Department of Biomedical Engineering

[3]Department of Chemical and Biological Engineering
Northwestern University, 2145 Sheridan Road, Evanston, IL 60208, USA

[4]Department of Chemistry, Faculty of Science, King Abdulaziz University, Jeddah 21589, Saudi Arabia

[5]Co-first author

[6]Lead Contact

*Correspondence: o-farha@northwestern.edu

http://dx.doi.org/10.1016/j.chempr.2016.05.001

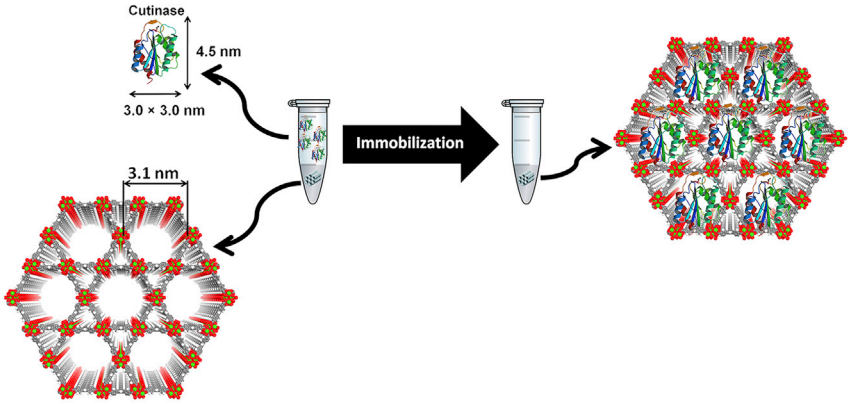

Figure 1. Immobilization of Cutinase in the Mesoporous Channels of NU-1000
Zr atoms are shown in green, C atoms are gray, O atoms are red, and H atoms are white.
See also Figure S1.

images (Figures 3C and 3D) indicate that the dye-labeled enzyme is in fact directed to the center of NU-1000 and that by decreasing the size of the particle from 10 to 1.5 μm, the time required to reach cutinase saturation is decreased by approximately 10-fold. We also modeled the diffusion process using Fick's second law in one dimension (Figures 3E and 3F). The best-fit value for the diffusion coefficient for Cut647 within NU-1000 was 2×10^{-13} cm^2/s, which is consistent with diffusive transport through the crystalline channels; the coefficient was found to be identical for 10 and 1.5 μm NU-1000 crystals. For comparison, the diffusion coefficient of cutinase on a 2D trimyristin support was found to be 8.0×10^{-10} cm^2/s.[36] These results suggest a strong interaction between Cut647 and NU-1000. In order to explain the nature of this strong interaction, we examined the zeta potential of NU-1000 with varying pH (Figure S2), which indicated an isoelectric point at approximately pH 4.3. This isoelectric point is consistent with our previous study on the Brønsted acidity of NU-1000.[37] Cutinase is known to have an isoelectric point at approximately pH 7.8.[38] Thus, in pH 7 buffer solution, cutinase and NU-1000 are positively and negatively charged, respectively. The strong interaction between Cut647 and NU-1000 can therefore be attributed to columbic forces.

We also used molecular mechanics calculations to computationally introduce a reported crystal structure of *F. solani pisi* cutinase into the hexagonal channels of NU-1000. The results indicated that in order to infiltrate the MOF, the long axis of the enzyme must orient along the mesoporous channel of NU-1000. In addition, the shape of cutinase changes slightly to allow for diffusion into the channels of NU-1000, resulting in an ellipsoid that is more elongated than the original cutinase structure (Figures 4A and S3). These models qualitatively support the small diffusion coefficients observed, as the enzyme must deform slightly to fit within the mesopore. In addition, the models indicate that the catalytically active site in cutinase, composed of amino acid residues Ser126, Asp180, and His194,[39] should remain accessible after encapsulation, with no indication of blocking by any framework components.

Cutinase Accessibility in NU-1000

One property of MOF-encapsulated enzymes that has yet to be explicitly addressed is the permeability of the crystals to small-molecule reactants after enzyme immobilization. We reasoned that the unique hierarchical pore structure of NU-1000 would

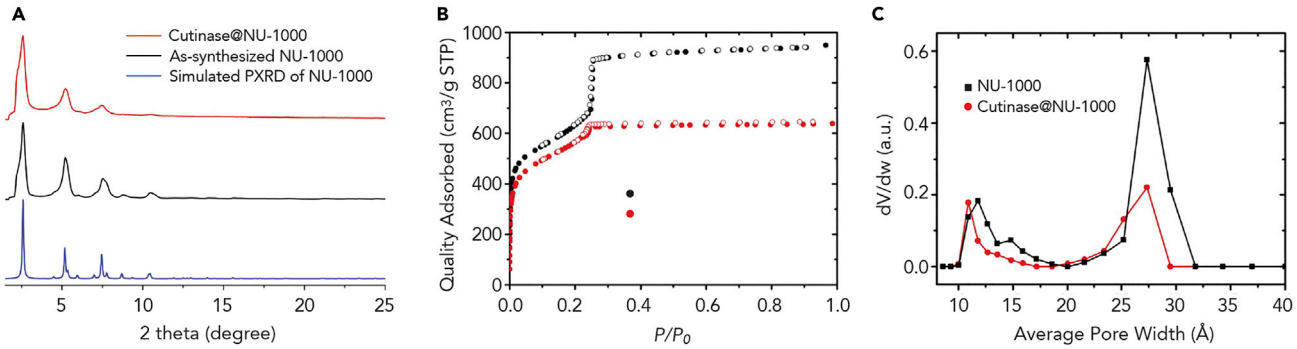

Figure 2. PXRD and N_2 Isotherms of Cutinase@NU-1000

(A) Simulated PXRD of NU-1000 (blue) and experimental PXRD of NU-1000 before (black) and after (red) cutinase loading.

(B) N_2 sorption isotherm of NU-1000 and cutinase@NU-1000 at 77 K.

(C) Pore-size distribution of as-synthesized NU-1000 and cutinase@NU-1000.

allow molecules of appropriate dimensions to diffuse into the interior of the crystal, even after enzyme encapsulation, either longitudinally via the triangular pore or laterally via the crystal windows. Molecules larger than either of these apertures should be excluded from the crystal due to blocking of the larger channels by cutinase. To test this idea, we chose two dye molecules (Figure 4B), one with dimensions small enough to diffuse through the smaller apertures (fluorescein: 1.0 × 0.8 × 0.5 nm, λ_{ex} = 488 nm, λ_{em} = 512 nm) and one too large to do so (4,4′,4″,4‴-(porphine-5,10,15,20-tetrayl)tetrakis(benzoic acid): 1.6 × 1.6 × 0.2 nm, λ_{ex} = 405 nm, λ_{em} = 640 nm), and compared the ability of each dye to permeate empty versus Cut647-loaded NU-1000-10 μm using CLSM. Both dyes have fluorescence emission maxima that lie well outside those of AlexaFluor 647. For empty NU-1000-10 μm, micrographs of samples immersed in solutions of fluorescein and porphyrin showed that both dyes can freely permeate the crystal (Figure S4). In the case of Cut647@NU-1000-10 μm, merged 3D reconstructions of z stacks from the 633 nm (dye-labeled cutinase) and 488 nm (fluorescein) laser channels showed the presence of Cut647 and that fluorescein retains access to the whole of the matrix (Figures 4C and S4). In the case of the larger porphyrin dye (UV 405 nm laser channel), we observed a size-exclusion effect whereby the molecule was blocked from entering the interior of the crystal and resided primarily on the surface (Figure 4D). This demonstrates that although the large hexagonal channels of NU-1000 are blocked by encapsulated cutinase, a reactant small enough to fit into the smaller triangular channels can still freely diffuse in and out of the framework.

Given that our computational model suggests that the active site of cutinase remains accessible after immobilization, we performed a real-time in situ CLSM experiment on cutinase@NU-1000-10 μm after the addition of a small aliquot of resorufin butyrate to determine whether the enzyme is accessible and active.[40] Enzymatic hydrolysis of resorufin butyrate by cutinase produces resorufin (λ_{ex} = 500 nm, λ_{em} = 593 nm), a highly fluorescent dye that can be used to monitor the catalytic activity of the encapsulated enzyme. When resorufin butyrate was added to a solid sample of cutinase@NU-1000-10 μm, the crystals of the MOF rapidly began to fluoresce at 593 nm throughout the crystal, indicating not only that the reactant reached the interior of the matrix but also that the encapsulated cutinase was accessible and reactive there. As the reaction proceeded, the fluorescence intensity of resorufin in solution increased, suggesting that the product can quickly diffuse out of the channels of NU-1000 (Movie S1). Control experiments using empty NU-1000-10 μm showed no

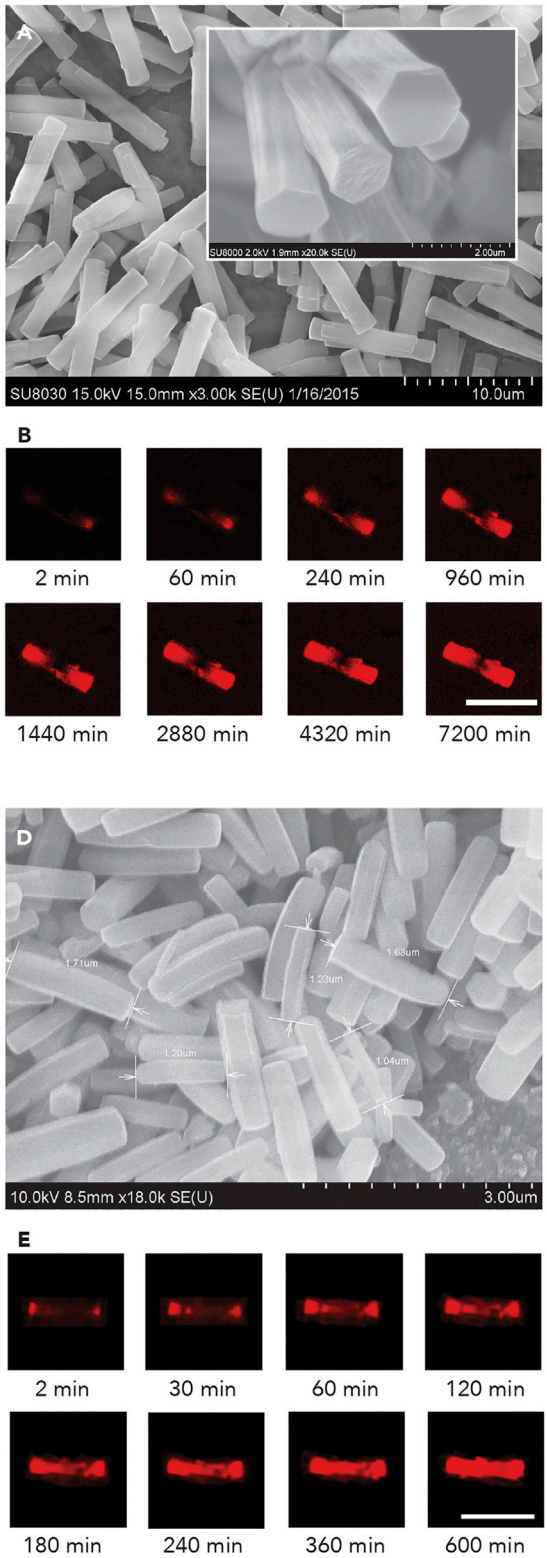

Figure 3. Diffusion Cut647 into NU-1000 Crystals with Different Lengths

(A and D) Scanning electron microscopy images of (A) 10 µm (inset image shows the typical hexagonal cylinder morphology of NU-1000 crystals) and (D) 1.5 µm.

Figure 3. *Continued*
(B and E) CLSM images of (B) a 10-μm NU-1000 crystal (scale bar represents 10 μm) and (E) a 1.5-μm NU-1000 crystal (scale bar represents 1.5 μm) after immersion in 100-μM Cut647 solution over time.
(C and F) An overlay of experimental Cut647 concentration (dots) and corresponding simulated fits (lines) along the middle of (C) a 10-μm NU-1000 crystal and (F) a 1.5-μm NU-1000 crystal at different time points.
See also Figure S1.

increase in fluorescence over the course of the experiment, indicating that the support has no catalytic activity of its own (Movie S2). To probe specifically the activity of enzymes sited in the MOF interior, we prepared a sample of NU-1000 containing active enzyme only in the interior of the crystal by treating NU-1000-10 μm with a 100 μM solution of cutinase for 2.5 hr followed by extensive washing. The sample was then placed in a 100 μM solution of catalytically inactive cutinase for 2 days to backfill the mesopores. In situ hydrolysis of resorufin butyrate was used to probe the enzyme accessibility and reactivity. We found that hydrolysis still occurred efficiently, indicating that reactant molecules can access cutinase not only on the MOF exterior but also in its crystalline interior (Figure 5 and Movie S3).

Activity and Stability of Immobilized Cutinase

Before testing the activity and stability of immobilized cutinase, we compared the hydrolysis of *p*-nitrophenyl butyrate (PNPB) using cutinase@NU-1000, NU-1000, and the final solution used to soak cutinase@NU-1000 as catalysts (Figure 6A). The results indicate there was no activity for NU-1000 and no active cutinase detectable in the final solution. To gain further insight into the influence of immobilization on activity, the enzyme kinetic parameters k_{cat} and K_M for free cutinase and cutinase@NU-1000-5 μm were determined for the hydrolysis of three representative substrates (esters offering different aliphatic chain lengths: *p*-nitrophenyl acetate [PNPA], PNPB, *p*-nitrophenyl octanoate [PNPO]) (Table S1 and Figure S5). The results suggest that immobilized cutinase has similar overall activity to free cutinase in solution. We next compared the stability of cutinase@NU-1000-5 μm relative to that of soluble cutinase under several challenging conditions. As a measure of stability, we monitored the catalytic hydrolysis of PNPB, a common esterase substrate, by the free and encapsulated enzyme (Figures 6B–6E) and compared the activity in terms of turnover number (TON) as summarized in Table S2. The activity was monitored: (1) in detergent-containing buffer, (2) detergent-free buffer, as well as in buffers containing (3) the denaturant urea, or (4) the organic solvent tetrahydrofuran (THF). Esterases that also hydrolyze lipids, such as cutinase, are known to show protein-concentration-dependent aggregation in the absence of detergents or stabilizing additives upon reaction with hydrophobic substrates.[41] In the buffer containing detergent, cutinase@NU-1000-5 μm and free cutinase showed comparable catalytic performance (Figure 6B). In buffer without detergent, however, solution-phase cutinase gradually lost its catalytic activity, whereas cutinase@NU-1000-5 μm maintained turnover (Figure 6C). In 30 min, the TON of cutinase@NU-1000-5 μm was almost twice that of free cutinase. In buffer solution containing urea (560 mM), soluble cutinase was completely deactivated after 5 min; in contrast, the catalytic activity of cutinase@NU-1000-5 μm was unchanged after 60 min (Figure 6D). The TON for cutinase@NU-1000-5 μm was almost five times that of free cutinase in 60 min. Similarly, in a buffer solution containing 2.5% THF, free cutinase was rapidly deactivated (8 min), whereas cutinase@NU-1000-5 μm was little affected (Figure 6E). Under these conditions, the TON for cutinase@NU-1000-5 μm was still five times that of free cutinase in 60 min. Finally, we tested the stability of the complex to

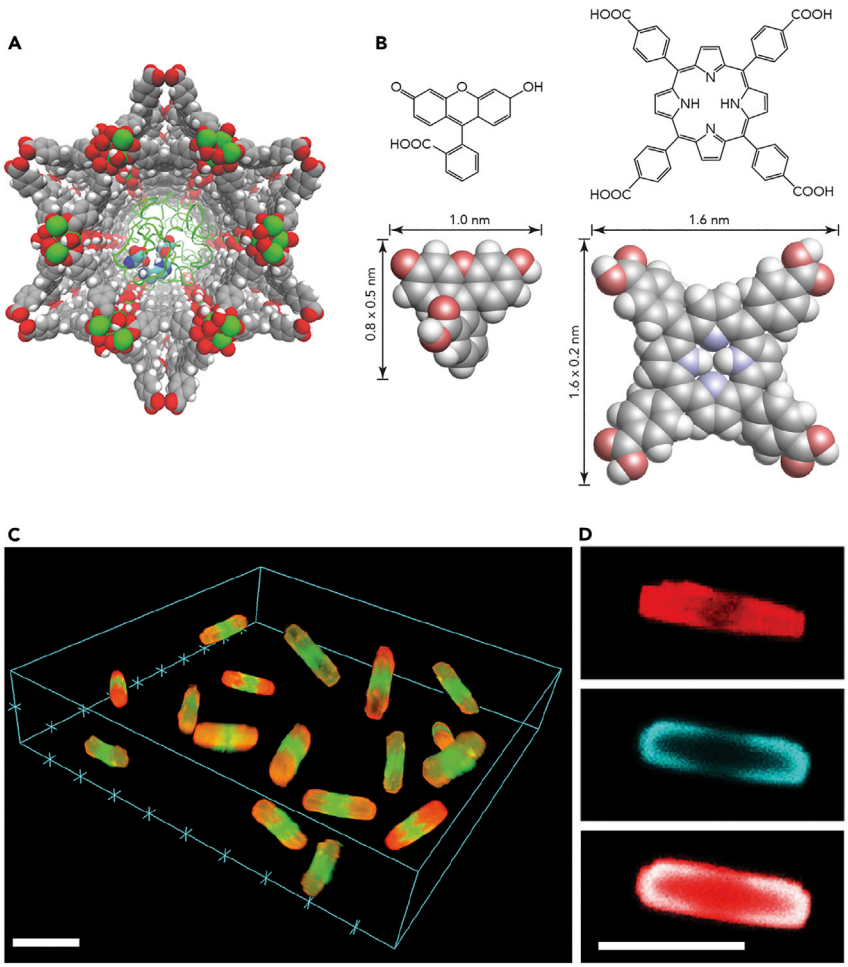

Figure 4. Simulation Model and Substrate Permeability of cutinase@NU-1000

(A) Model of cutinase@NU-1000 after geometry optimization (NU-1000 and the active triad of cutinase-Ser126, Asp180, and His194 are displayed in a CPK model; Zr atoms are shown in green, C atoms are gray, O atoms are red, N atoms are blue, and H atoms are white).

(B) Dye molecules fluorescein and 4,4′,4″,4‴-(porphine-5,10,15,20-tetrayl)tetrakis(benzoic acid) (TCPP) used to test reactant diffusion in cutinase@NU-1000-10 μm.

(C) 3D reconstructed image of Cut647@NU-1000-10 μm crystals containing fluorescein (scale bar represents 10 μm).

(D) 2D CLSM images taken using different laser channels to view Cut647, TCPP, and both Cut647 and TCPP in a single NU-1000-10 μm crystal (red for Cut647, green for fluorescein, and blue for TCPP; scale bar represents 10 μm).

See also Figures S3 and S4.

repeated reaction by following the hydrolysis of 300 μM PNPB catalyzed by 20 μg cutinase@NU-1000-5 μm over five reaction cycles. After each cycle, the complex was isolated by centrifugation, washed extensively with buffer, and subjected to another round of reaction. After five cycles, around 60% of the catalytic activity of cutinase@NU-1000-5 μm was retained (Figure 6F).

Comparing the Accessibility of Cutinase Immobilized in NU-1000 versus Other MOF Supports

We compared the activity of cutinase immobilized in representative channel-type mesoporous MOFs to investigate the role of the unique hierarchical structure of NU-1000 for enzyme encapsulation applications. CYCU-3[42] and PCN-600[43]

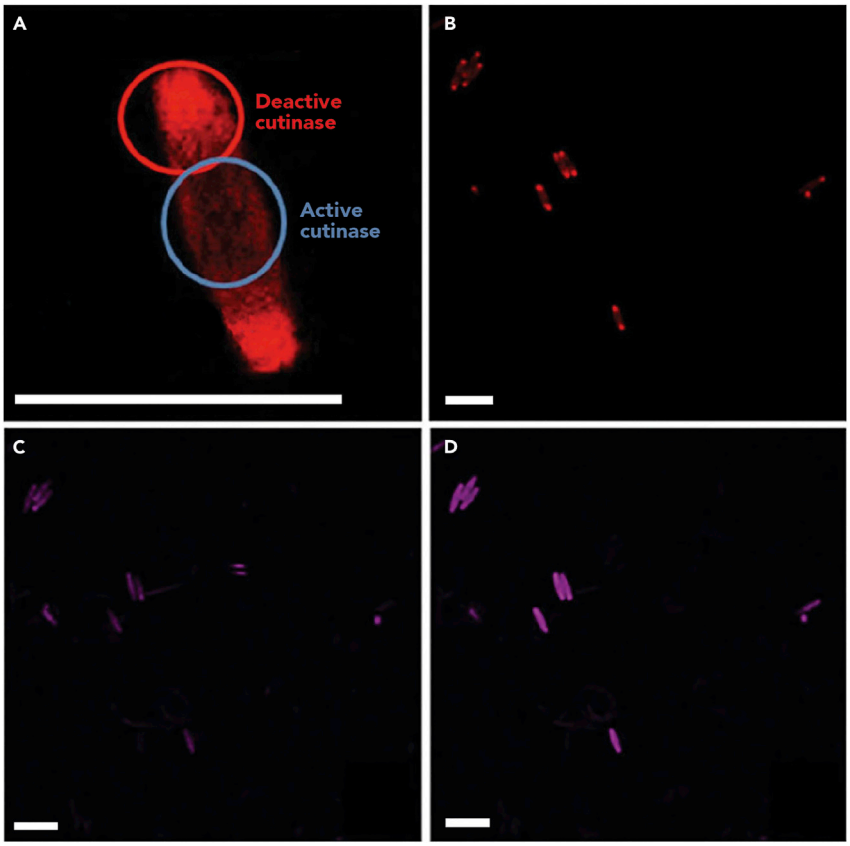

Figure 5. In Situ Hydrolysis of Resorufin by Blocked cutinase@NU-10000

CLSM images of (A) a magnified image of a single NU-1000-10 μm crystal containing active cutinase (highlighted in a blue circle, not labeled with AlexaFluor 647) blocked by deactivated cutinase (highlighted in a red circle, labeled with AlexaFluor 647) and (B) multiple crystals of NU-1000 showing active and deactivated cutinase similar to the image in Figure 7A. In situ hydrolysis of resorufin butyrate using cutinase@NU-1000 containing active and deactivated cutinase for (C) 5 s and (D) 60 s in buffer solution at room temperature. Scale bars represent 10 μm. See also Movie S3.

were chosen as control MOFs to compare with NU-1000 (Figure 7A). All of these channel-type MOFs possess mesopores approximately 3.0 nm in diameter but differ in the identity of the metal nodes, organic linkers, and connectivity, resulting in different channel systems and accessibility within these frameworks. PCN-600 contains only hexagonal mesopores, which can, however, communicate via channel windows. CYCU-3 features a hierarchical micro-mesopore architecture similar to NU-1000; however, the walls of the channels in CYCU-3 are too condensed to allow reactant to diffuse freely between neighboring channels. In contrast, NU-1000 has open windows between the microporous and mesoporous channels, allowing for free communication between the different-sized pores. To observe the diffusion of cutinase into PCN-600 and CYCU-3, micro-sized crystals of each MOF were prepared for comparison with NU-1000-5 μm, and the loading of Cut647 in these MOFs was followed by CLSM over 5 days (Figure S6). The diffusion behavior of cutinase in all three MOFs was similar; cutinase slowly diffused from the two ends of each crystal into the center of the MOF. This demonstrates the generality of immobilization of enzymes into channel-type MOFs. To compare enzyme accessibility in CYCU-3, PCN-600, and NU-1000, nano-sized crystals of these three

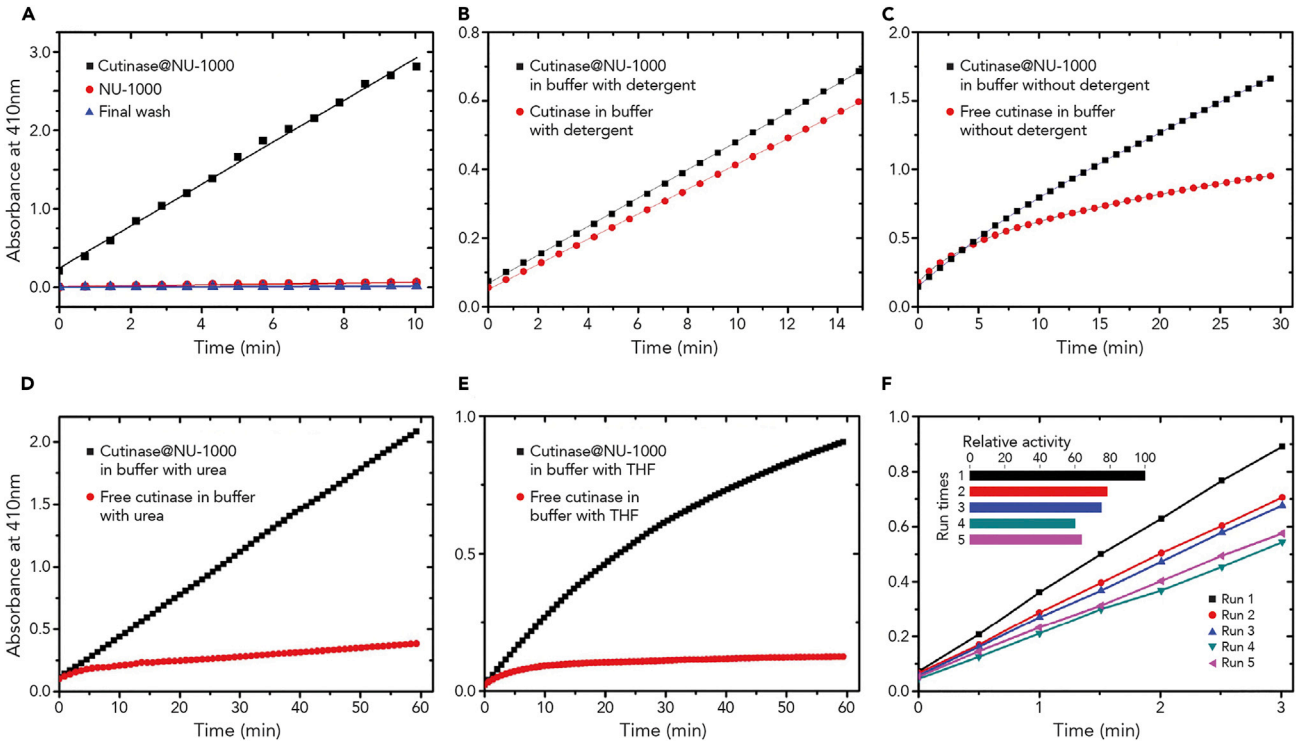

Figure 6. Activity and Stability Assays

(A–E) Reaction kinetics of PNPB hydrolysis by cutinase@NU-1000 (black), NU-1000 (red), and the supernatant solution used to soak cutinase@NU-1000 (blue). Kinetic study of hydrolysis of PNPB by (A) cutinase@NU-1000 (black) and free cutinase (red) in (B) buffer with detergent, (C) buffer without detergent, (D) buffer with urea, and (E) buffer with THF.

(F) Recyclability test of cutinase@NU-1000 in buffer without detergent.

MOFs were synthesized[44] to ensure that the rate of diffusion was maximized and that the maximum loading of cutinase in each framework was achieved within 24 hr (Figure S6A). The final amounts of cutinase encapsulated by nano-sized NU-1000, CYCU-3, and PCN-600 were 12.9, 9.8, and 24.5 nmol/mg, respectively, as determined by ICP-OES. These findings are broadly consistent with the available mesopore volumes, i.e., ~0.95 cm^3/g for NU-1000 versus 0.90 cm^3/g for CYCU-3 and 1.80 cm^3/g for PCN-600. To ensure complete removal of any enzyme immobilized on the external surface of each nano-sized MOF prior to accessibility testing, the proteolytic agent trypsin was used to decompose cutinase on the outer surface (Figure 7B). The dimensions of trypsin are similar to those of cutinase, and thus cutinase sited within the MOF should not be decomposed by this process. The percentages of cutinase removed from the exteriors of NU-1000, CYCU-3, and PCN-600 were 3%, 39%, and 2%, respectively (Figure 7C). The comparatively large percentage of cutinase removed from CYCU-3 can be attributed to its comparatively poor stability in water, and therefore CYCU-3 was not studied further.

To accurately evaluate the accessibility of cutinase after immobilization in NU-1000 versus PCN-600, an organophosphorus ester with a fluorescent resorufin group was synthesized and used as an active-site titrant (Figures S7 and S8).[45] The titration results show that in PCN-600, only 1.5 nmol/mg (6% of the total amount) of cutinase encapsulated in the channels showed activity. Given that PCN-600

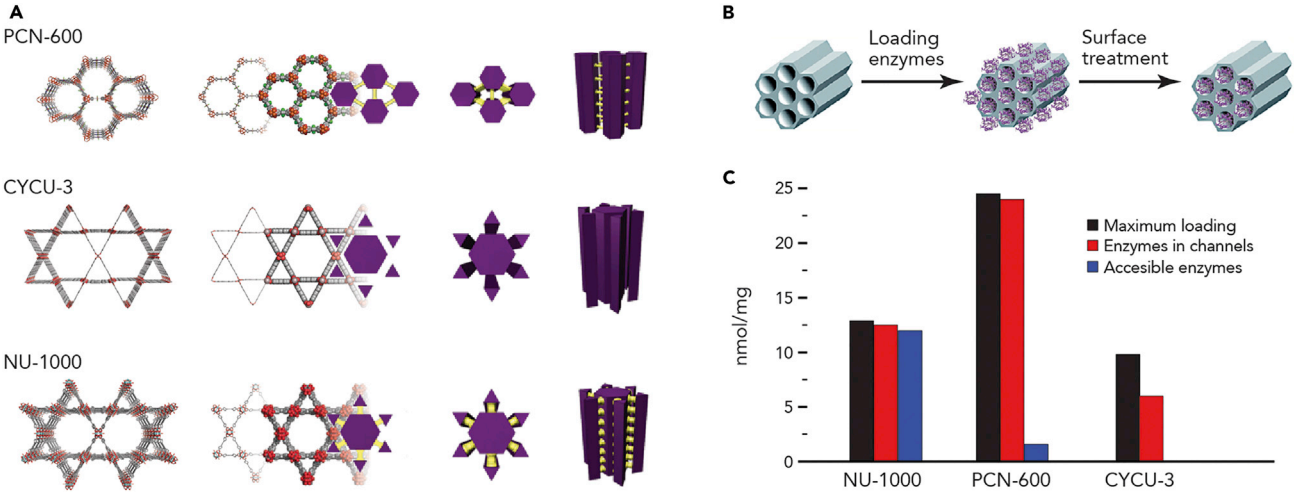

Figure 7. Active-Site Accessibility of Immobilized Cutinases in MOFs

(A) Perspective view of 1D channels of PCN-600, CYCU-3, and NU-1000. Purple cylinders represent the channels, and yellow tunnels indicate the connectivity between neighboring channels.

(B) Schematic of the enzyme-loading and surface-treatment process.

(C) Maximum loading capacity (black), enzymes encapsulated in channels (red), and accessible enzymes (blue) in nano-sized MOFs.

See also Figures S6–S8.

contains only hexagonal mesoporous channels, this result is not surprising because many of the mesopores are expected to be blocked by encapsulated cutinase, leaving little room for reactant diffusion. On the other hand, in NU-1000, 93% of the encapsulated cutinase was found to be accessible and catalytically active (Figure 7C). This demonstrates that, in addition to the importance of hierarchical pore structure for reactant diffusion, the presence of windows between the pores is key to achieving enzyme accessibly and hence enzyme turnover in a solid support.

Conclusions

By immobilizing an enzyme in the water-stable, hierarchical, channel-type MOF NU-1000, the enzyme can be stabilized in the array of larger channels, and reactants and products can diffuse through the array of smaller channels in the framework. It is this integration of large and small channels with the windows that connect them throughout the crystal that allows the MOF to be optimized for both binding and stabilization of the enzyme and diffusion of reactants and products. We have shown that NU-1000 is an excellent support for stabilizing the encapsulated enzyme in varying media such as THF and urea, whereas the free enzyme degrades rapidly under these conditions. Considering this stabilization of the enzyme, active-site accessibility, and open structure for diffusion, the design of channel-type mesoporous MOFs with hierarchical pore structure and pore windows should inspire further investigation in enzyme immobilization applications for biocatalysis where high catalytic efficiency and enhanced stability are required. Relevant to studies with other enzymes, and to optimization of enzyme activity, the degree of channel hydrophobicity in NU-1000 has been found to be highly tunable, as has the (bio)chemical composition of the channel lining, e.g., fluorocarbons, polypeptides, organic acids and bases, luminescent dyes, and even metal-sulfide clusters.[46,47] The tunability of MOFs, along with our increasing

understanding of the design rules for stabilizing enzymes in an accessible fashion, hold great promise for the immobilization of an ever-expanding array of useful enzyme catalysts.

EXPERIMENTAL PROCEDURES

Materials

Zirconyl chloride octahydrate ($ZrOCl_2 \cdot 8H_2O$), benzoic acid (C_6H_5COOH), aluminum chloride nonahydrate ($AlCl_3 \cdot 9H_2O$), *N*,*N*-dimethylformamide, trifluoroacetic acid, 4,4′-stilbenedicarboxylic acid (H_2SDC), PNPA, PNPB, PNPO, diethyl butylphosphonate, tris(hydroxymethyl)aminomethane (Tris), citric acid, fluorescein, resorufin butyrate, and resorufin sodium salt were purchased from Sigma-Aldrich and used as received. Fe(III) meso-tetra(4-carboxyphenyl)porphine chloride (FeTCPP) and meso-tetra(4-carboxyphenyl)porphine (TCPP) were purchased from Frontier Scientific and used without further purification. Iron(III) nitrate nonahydrate ($Fe(NO_3)_3 \cdot 9H_2O$) and sodium acetate trihydrate ($NaOOCCH_3 \cdot 3H_2O$) were purchased from Alfa Aesar. AlexaFluor 647 dye was purchased from Life Technologies (Thermo Fisher Scientific). The ligand 1,3,6,8-tetrakis(*p*-benzoic acid)pyrene (H_4TBAPy) was synthesized according to the published procedure.[29] NU-1000, CYCU-3, precursor [$Fe_3O(OOCCH_3)_6OH$], and PCN-600 were synthesized according to published procedures.[42–44] *F. solani pisi* cutinase (molecular weight, 22.5 kDa) was made and purified according to a protocol described elsewhere.[32] Buffered aqueous solutions of cutinase (10^{-5}–10^{-7} M) were prepared at pH values of 6 (citric acid buffer) and 7.4 (Tris-HCl buffer).

PXRD

PXRD data were collected on a Rigaku model ATX-G diffractometer equipped with a Cu rotating anode X-ray source. This work made use of the J.B. Cohen X-Ray Diffraction Facility, supported by the Materials Research Science and Engineering Center (MRSEC) program of the National Science Foundation (NSF, DMR-1121262) at the Materials Research Center of Northwestern University.

Measurements of Gas Adsorption

N_2 sorption isotherm measurements were performed on a Micromeritics Tristar II 3020 (Micromeritics) at 77 K. Between 30 and 100 mg of material was used for each measurement.

Scanning Electron Microscopy

Scanning electron microscopy images were taken using a Hitachi SU8030 or a Hitachi S4800-II at the EPIC facility (Atomic and Nanoscale Characterization Experimental Center, Northwestern University), which has received support from the MRSEC program (NSF DMR-1121262) at the Materials Research Center, the Nanoscale Science and Engineering Center (NSF EEC-0647560) at the International Institute for Nanotechnology, and the State of Illinois through the International Institute for Nanotechnology.

NMR Spectroscopy

^1H and ^{13}C nuclear magnetic resonance (NMR) spectra were recorded on a Bruker 500 FT-NMR spectrometer (500 MHz for ^1H and 126 MHz for ^{13}C), and ^{31}P NMR spectra were recorded on an Agilent 400 FT-NMR spectrometer (400 MHz) at the IMSERC (Integrated Molecular Structure Education and Research Center) of Northwestern University.

Electrospray Ionization Mass Spectrometry

Data from electrospray ionization mass spectrometry were recorded on a Bruker AmaZon SL Ion Trap at the IMSERC.

Measurement of Zeta Potential

The zeta potential of samples was measured using a Malvern Zetasizer Nano ZS. NU-1000 samples were made up in 18.2 MΩ deionized water at a concentration of 0.1 mg/ml and sonicated for 15 min. The pH of the solution was manually adjusted from 3 to 8 by the addition of 0.1 M HCl or NaOH to 10–15 ml of the suspension before the zeta potential was measured.

ICP-OES Analysis

Quantification of zirconium (Zr) and sulfur (S) was accomplished using ICP-OES of acid-digested samples using individual Zr and S elemental standards prepared by diluting a 10,000 ppm certified Zr standard and 10,000 ppm certified S standard (Ricca Chemical Company) to 1.5625, 3.125, 6.25, 12.5, 25, and 50 ppm concentrations with 3% nitric acid (v/v), up to a total sample volume of 10 ml. ICP-OES was performed on a computer-controlled (QTEGRA software v.2.2) Thermo iCap 7600 Duo ICP-OES (Thermo Fisher Scientific) operating in standard mode and equipped with a SPRINT valve and CETAC 520 autosampler (Teladyne CETAC). Each sample was acquired using a 5 s sample loop fill (4 ml sample loop), a 4 s loop rinse, and a 4 s extra loop rinse (the rinse was 2% HNO_3 [v/v] and 2% HCl [v/v]). Samples were analyzed for Zr in radial view (339.198, 343.823, and 327.305 nm wavelengths) and S in axial view (180.731, 182.034, and 182.624 nm wavelengths) with three replicates and an exposure time of 20 s. Instrument performance was verified weekly via a performance report (passing manufacturer specifications). The enzyme loading was determined by comparing the experimental Zr/S ratio to the theoretical ratio given by the stoichiometry of Zr in the MOF to the number of cysteine thiols present in cutinase (Zr/S = 96:1).

General Procedure for Kinetic Study of the Hydrolysis Reaction

Hydrolysis profiles of PNPA, PNPB, and PNPO by using cutinase or immobilized cutinase were recorded on a Beckman Coulter DU 640 spectrophotometer. Stock solutions of the esters were prepared using DMSO as a diluent. NU-1000-immobilized cutinase suspensions and free cutinase solution concentrations were adjusted to give similar initial rate profiles and time course length before treatment with various substrate concentrations. The reactions were conducted in a 1 ml cuvette containing 10 μl of the ester stock solution, 10 μl of enzyme solution/MOF-enzyme complex suspension, and 980 μl of TBS + 0.1% Triton X-100. Absorbance data at 410 nm (*p*-nitrophenyl absorption) were collected versus time. Michealis parameters for the enzyme substrate reactions were obtained using Lineweaver-Burke analysis of the initial rate data.

Stability and Recyclability Test

The stability of 5 nM cutinase and 5 nM immobilized cutinase in NU-1000 were compared using PNPB as a reactant in different media. For the recycling studies with NU-1000-immobilized cutinase, the reaction was performed with 300 μM PNPB using 20 μg of cutinase@NU-1000-5 μm in Tris buffer at pH 7 and room temperature. After the reaction, the mixture was centrifuged, and the supernatant was separated. The resulting solid was washed three times with Tris buffer to remove any soluble residue. The recovered NU-1000-immobilized cutinase was used for the next reaction by adding the same amount of reactant and buffer. The procedure was repeated five times as described above. The relative activity was calculated as a

ratio of the enzyme activity at any given cycle versus the enzyme activity during the first cycle.

Labeling Cutinase with Fluorescent Dye

AlexaFluor 647-labeled cutinase (Cut647) was prepared by reacting cutinase (100 μM) with 1.2 equivalents of an AlexaFluor 647-(ethyl-*p*-nitrophenyl)-phosphonate conjugate followed by purification of the labeled protein by size-exclusion chromatography.[48] This rendered the enzyme catalytically inactive. AlexaFluor 647 was chosen because of the relative insensitivity of its fluorescence intensity and quantum yield to environmental conditions and because of the excitation and emission maxima (650 and 665 nm, respectively) that occur far outside that of the pyrene struts (390 and 471/529 nm) used to construct the MOF. In the CLSM experiment using deactivated cutinase (Cut647), the complete loss of hydrolysis activity was confirmed by PNPB activity assay.

Immobilization of Cutinase in MOFs

2 mg of activated MOF (NU-1000, PCN-600, or CYCU-3) was added to 1 ml of deionized water and sonicated for 5 min until a uniform suspension was formed. The well-dispersed solid was isolated by centrifugation at 15,000 rpm for 1 min, and the supernatant was decanted. The solid was then suspended in a solution of cutinase (500 μl, 100 μM) in TBS (pH 7.4) for a given time (1 day for nano-sized MOF and 5 days for micro-sized MOF) at 25°C. The MOF-cutinase composite was then isolated by centrifugation at 15,000 rpm for 1 min, and the supernatant was removed. The solid was washed five times more with TBS containing 0.1% Triton X-100 and soaked in TBS buffer solution before further experiments.

CLSM Analysis

NU-1000-10 μm crystals were used for all CLSM studies to monitor the uptake of cutinase and the distribution of enzymes throughout the matrix.[49] Fluorescence was examined by applying CLSM on a Leica TCS SP5. The Ar laser was set to 5%. Bit depth was set to 12 to achieve intensity resolution of 4,096 gray levels. Laser line 633 with 3% laser power was used to visualize AlexaFluor 647-dye-labeled cutinase on NU-1000. Quantitative analyses were performed using Leica LAS-AF image analysis, where a region of interest (ROI) was manually selected using the line tool. In a selected ROI, measurements of the relative mean intensity of the fluorescence signals were taken by the Leica LAS-AF image analysis program. The Mark and Find panel was used to locate the position (x, y, and z coordinates) of the same single crystal of NU-1000 during the test at different time points. The loading process of Cut647 into a single crystal of NU-1000 was monitored using in situ CLSM. The submerged NU-1000 crystals were first placed into a solution with Tris buffer. 2D (xy) concentration profiles of Cut647 taken at a fixed z depth (corresponding to the center layer) within the crystal of NU-1000 were acquired on a Leica-SP5 CLSM once Cut647 was added to the solution. During imaging, the laser power was set as low as possible (5%, 1 mW HeNe laser) to avoid fluorescence saturation and to minimize photo bleaching. To obtain time-dependent Cut647 concentration profiles for the MOF and avoid decay of the fluorophore caused by repeated illumination by the laser, images were acquired only at given time intervals: 2, 60, 240, 960, 1,440, 2,880, 4,320, and 7,200 min. Using the line tool in ImageJ,[50] fluorescence intensity profiles along the middle of an NU-1000 crystal were obtained for each sample and plotted as a function of the length of the crystal versus time.

Titration of Active Sites for Cutinase and Immobilized Cutinase in MOFs

The titration experiments were performed using the Molecular Devices Gemini EM fluorescence/chemiluminescence plate reader. A calibration curve relating cutinase activity to the intensity of liberated resorufin was generated by treating cutinase at several concentrations (8 μM, 6 μM, 4 μM, 2 μM, 1 μM, and 500 nM) in 4-morpholineethanesulfonic acid (MES)-saline buffer (20 mM MES, 150 mM NaCl [pH 6.0]) with a solution of 5 μM resorufin phosphonate (RP) in MES-saline at 37°C. Steady-state fluorescence intensities at the completion of the reaction were plotted versus enzyme concentration and fitted to a straight line to generate the calibration curve. For the titration experiments, 5 μg of nano-sized empty NU-1000, empty PCN-600, cutinase@NU-1000, and cutinase@PCN-600 were treated with RP (5 μM) at 37°C, and the fluorescence intensity was monitored for 5 hr. Background-subtracted steady-state fluorescence values for each of the experimental samples were then compared with the calibration curve to yield the concentration of cutinase active sites present in the MOF-enzyme samples.

SUPPLEMENTAL INFORMATION

Supplemental Information includes Supplemental Experimental Procedures, eight figures, two tables, and three movies and can be found with this article online at http://dx.doi.org/10.1016/j.chempr.2016.05.001.

AUTHOR CONTRIBUTIONS

O.K.F., J.T.H., and M.M. initiated the project; P.L. (with some help from A.J.H.) synthesized the MOF and collected and analyzed the data from gas adsorption, X-ray diffraction, scanning electron microscopy, CLSM, ICP-OES, and NMR under the supervision of O.K.F. and J.T.H.; J.A.M. prepared the enzymes, labeled the enzymes with dyes, and performed the titration experiments under the supervision of M.M.; E.V. and P.Z.M. performed the computations and analyzed the results under the supervision of R.Q.S.; P.L., J.A.M., and A.J.H. wrote the paper, and all authors contributed to revising the paper.

ACKNOWLEDGMENTS

O.K.F., J.T.H., and R.Q.S. gratefully acknowledge DTRA for financial support (HDTRA1-14-1-0014), and M.M. acknowledges the AFOSR (FA9550-16-1-0150). The authors thank Dr. Brian Pate (Joint Science & Technology Office for Chemical & Biological Defense, Defense Threat Reduction Agency) for helpful discussions and Jessica Hornick and Dr. Keith MacRenaris for helpful discussions on CLSM and ICP-OES experiments, respectively. We also thank Dr. Nicolaas A. Vermeulen for designing and producing the MOF graphs. Imaging work was done at the Northwestern University Biological Imaging Facility, generously supported by the NU Office for Research. Confocal microscopy was performed on a Leica TCS SP5 laser scanning confocal microscope system purchased with funds from the NU Office for Research. ICP-OES analysis was performed at the Northwestern University Quantitative Bio-element Imaging Center, generously supported by a NASA Ames Research Center grant (NNA04CC36G).

Received: March 17, 2016
Revised: April 25, 2016
Accepted: May 19, 2016
Published: June 9, 2016

REFERENCES AND NOTES

1. Bornscheuer, U.T., Huisman, G.W., Kazlauskas, R.J., Lutz, S., Moore, J.C., and Robins, K. (2012). Engineering the third wave of biocatalysis. Nature *485*, 185–194.

2. Sheldon, R.A., and van Pelt, S. (2013). Enzyme immobilisation in biocatalysis: why, what and how. Chem. Soc. Rev. *42*, 6223–6235.

3. Vidinha, P., Augusto, V., Almeida, M., Fonseca, I., Fidalgo, A., Ilharco, L., Cabral, J.M., and Barreiros, S. (2006). Sol-gel encapsulation: an efficient and versatile immobilization technique for cutinase in non-aqueous media. J. Biotechnol. *121*, 23–33.

4. Melo, E.P., Faria, T.Q., Martins, L.O., Goncalves, A.M., and Cabral, J.M.S. (2001). Cutinase unfolding and stabilization by trehalose and mannosylglycerate. Proteins *42*, 542–552.

5. Deng, H., Grunder, S., Cordova, K.E., Valente, C., Furukawa, H., Hmadeh, M., Gándara, F., Whalley, A.C., Liu, Z., Asahina, S., and Kazumori, H. (2012). Large-pore apertures in a series of metal-organic frameworks. Science *336*, 1018–1023.

6. Lykourinou, V., Chen, Y., Wang, X.S., Meng, L., Hoang, T., Ming, L.J., Musselman, R.L., and Ma, S. (2011). Immobilization of MP-11 into a mesoporous metal-organic framework, MP-11@mesoMOF: a new platform for enzymatic catalysis. J. Am. Chem. Soc. *133*, 10382–10385.

7. Feng, D., Liu, T.F., Su, J., Bosch, M., Wei, Z., Wan, W., Yuan, D., Chen, Y.P., Wang, X., Wang, K., and Lian, X. (2015). Stable metal-organic frameworks containing single-molecule traps for enzyme encapsulation. Nat. Commun. *6*, 5979.

8. Chen, Y., Lykourinou, V., Vetromile, C., Hoang, T., Ming, L.J., Larsen, R.W., and Ma, S. (2012). How can proteins enter the interior of a MOF? Investigation of cytochrome c translocation into a MOF consisting of mesoporous cages with microporous windows. J. Am. Chem. Soc. *134*, 13188–13191.

9. Shieh, F.K., Wang, S.C., Yen, C.I., Wu, C.C., Dutta, S., Chou, L.Y., Morabito, J.V., Hu, P., Hsu, M.H., Wu, K.C.W., and Tsung, C.K. (2015). Imparting functionality to biocatalysts via embedding enzymes into nanoporous materials by a de novo approach: size-selective sheltering of catalase in metal-organic framework microcrystals. J. Am. Chem. Soc. *137*, 4276–4279.

10. Lyu, F., Zhang, Y., Zare, R.N., Ge, J., and Liu, Z. (2014). One-pot synthesis of protein-embedded metal–organic frameworks with enhanced biological activities. Nano Lett. *14*, 5761–5765.

11. Liang, K., Ricco, R., Doherty, C.M., Styles, M.J., Bell, S., Kirby, N., Mudie, S., Haylock, D., Hill, A.J., Doonan, C.J., and Falcaro, P. (2015). Biomimetic mineralization of metal-organic frameworks as protective coatings for biomacromolecules. Nat. Commun. *6*, 7240.

12. Furukawa, H., Cordova, K.E., O'Keeffe, M., and Yaghi, O.M. (2013). The chemistry and applications of metal-organic frameworks. Science *341*, 1230444.

13. Li, J.R., Kuppler, R.J., and Zhou, H.C. (2009). Selective gas adsorption and separation in metal-organic frameworks. Chem. Soc. Rev. *38*, 1477–1504.

14. Mason, J.A., Veenstra, M., and Long, J.R. (2014). Evaluating metal-organic frameworks for natural gas storage. Chem. Sci. *5*, 32–51.

15. Peng, Y., Krungleviciute, V., Eryazici, I., Hupp, J.T., Farha, O.K., and Yildirim, T. (2013). Methane storage in metal-organic frameworks: current records, surprise findings, and challenges. J. Am. Chem. Soc. *135*, 11887–11894.

16. So, M.C., Wiederrecht, G.P., Mondloch, J.E., Hupp, J.T., and Farha, O.K. (2015). Metal-organic framework materials for light-harvesting and energy transfer. Chem. Commun. *51*, 3501–3510.

17. Wang, J.L., Wang, C., and Lin, W.B. (2012). Metal-organic frameworks for light harvesting and photocatalysis. ACS Catal. *2*, 2630–2640.

18. Williams, D.E., and Shustova, N.B. (2015). Metal–organic frameworks as a versatile tool to study and model energy transfer processes. Chem. Eur. J. *21*, 15474–15479.

19. Horcajada, P., Serre, C., Vallet-Regí, M., Sebban, M., Taulelle, F., and Férey, G. (2006). Metal-organic frameworks as efficient materials for drug delivery. Angew. Chem. Int. Ed. Engl. *45*, 5974–5978.

20. Lee, J., Farha, O.K., Roberts, J., Scheidt, K.A., Nguyen, S.T., and Hupp, J.T. (2009). Metal-organic framework materials as catalysts. Chem. Soc. Rev. *38*, 1450–1459.

21. Barreira, G., Ferreira, A.S., Vidinha, P., Cabral, J.M., Martinho, J.M., Lima, J.C., Cabrita, E.J., and Barreiros, S. (2014). Assessing diffusion in enzyme loaded sol-gel matrices. RSC Adv *4*, 25099–25105.

22. Scherer, R., Oliveira, J.V., Pergher, S., and de Oliveira, D. (2011). Screening of supports for immobilization of commercial porcine pancreatic lipase. Mat. Res. *14*, 483–492.

23. Hartmann, M. (2005). Ordered mesoporous materials for bioadsorption and biocatalysis. Chem. Mater. *17*, 4577–4593.

24. Yasutaka, K., Takato, Y., Takashi, K., Kohsuke, M., and Hiromi, Y. (2011). Enhancement in adsorption and catalytic activity of enzymes immobilized on phosphorus- and calcium-modified MCM-41. J. Phys. Chem. B *115*, 10335–10345.

25. Zou, B., Hu, Y., Jiang, L., Jia, R., and Huang, H. (2013). Mesoporous material SBA-15 modified by amino acid ionic liquid to immobilize lipase via ionic bonding and cross-linking method. Ind. Eng. Chem. Res. *52*, 2844–2851.

26. Mateo, C., Palomo, J.M., Fernandez-Lorente, G., Guisan, J.M., and Fernandez-Lafuente, R. (2007). Improvement of enzyme activity, stability and selectivity via immobilization techniques. Enzyme Microb. Technol. *40*, 1451–1463.

27. Sheldon, R.A. (2007). Enzyme immobilization: the quest for optimum performance. Adv. Synth. Catal. *349*, 1289–1307.

28. Hudson, S., Cooney, J., and Magner, E. (2008). Proteins in mesoporous silicates. Angew. Chem. Int. Ed. Engl. *47*, 8582–8594.

29. Mondloch, J.E., Bury, W., Fairen-Jimenez, D., Kwon, S., DeMarco, E.J., Weston, M.H., Sarjeant, A.A., Nguyen, S.T., Stair, P.C., Snurr, R.Q., Farha, O.K., and Hupp, J.T. (2013). Vapor-phase metalation by atomic layer deposition in a metal–organic framework. J. Am. Chem. Soc. *135*, 10294–10297.

30. De Barros, D.P., Fonseca, L., Cabral, J.M., Weiss, C.K., and Landfester, K. (2009). Synthesis of alkyl esters by cutinase in miniemulsion and organic solvent media. Biotechnol. J. *4*, 674–683.

31. Dutta, K., and Dasu, V.V. (2011). Synthesis of short chain alkyl esters using cutinase from *Burkholderia cepacia* NRRL B2320. J. Mol. Catal. B Enzym. *72*, 150–156.

32. Chen, S., Su, L., Chen, J., and Wu, J. (2013). Cutinase: characteristics, preparation, and application. Biotechnol. Adv. *31*, 1754–1767.

33. Nyyssölä, A. (2015). Which properties of cutinases are important for applications? Appl. Microbiol. Biotechnol. *99*, 4931–4942.

34. Santos, A.M., Fedorov, A., Martinho, J.M., Baptista, R.P., Taipa, M.Â., and Cabral, J.M. (2008). Orientation of cutinase adsorbed onto PMMA nanoparticles probed by tryptophan fluorescence. J. Phys. Chem. B *112*, 3581–3585.

35. Mondloch, J.E., Katz, M.J., Isley, W.C., III, Ghosh, P., Liao, P., Bury, W., Wagner, G.W., Hall, M.G., DeCoste, J.B., Peterson, G.W., Snurr, R.Q., Cramer, C.J., Hupp, J.T., and Farha, O.K. (2015). Destruction of chemical warfare agents using metal–organic frameworks. Nat. Mater. *14*, 512–516.

36. Sonesson, A.W., Elofsson, U.M., Callisen, T.H., and Brismar, H. (2007). Tracking single lipase molecules on a trimyristin substrate surface using quantum dots. Langmuir *23*, 8352–8356.

37. Klet, R.C., Liu, Y., Wang, T.C., Hupp, J.T., and Farha, O.K. (2016). Evaluation of Brønsted acidity and proton topology in Zr-and Hf-based metal–organic frameworks using potentiometric acid–base titration. J. Mater. Chem. A *4*, 1479–1485.

38. Petersen, S.B., Fojan, P., Petersen, E.I., and Petersen, M.T.N. (2001). The thermal stability of the *Fusarium solani pisi* cutinase as a function of pH. J. BioMed. Biotechnol. *1*, 62–69.

39. Liu, Z., Gosser, Y., Baker, P.J., Ravee, Y., Lu, Z., Alemu, G., Li, H., Butterfoss, G.L., Kong, X.P., Gross, R., and Montclare, J.K. (2009). Structural and functional studies of *Aspergillus oryzae* cutinase: enhanced thermostability and hydrolytic activity of synthetic ester and polyester degradation. J. Am. Chem. Soc. *131*, 15711–15716.

40. Lam, V., Henault, M., Khougaz, K., Fortin, L.J., Ouellet, M., Melnyk, R., and Partridge, A. (2012). Resorufin butyrate as a soluble and monomeric high-throughput substrate for a triglyceride lipase. J. Biomol. Screen. *17*, 245–251.

41. Pedersen, S., Nesgaard, L., Baptista, R.P., Melo, E.P., Kristensen, S.R., and Otzen, D.E.

(2006). PH-dependent aggregation of cutinase is efficiently suppressed by 1, 8-ANS. Biopolymers *83*, 619–629.

42. Lo, S.H., Chien, C.H., Lai, Y.L., Yang, C.C., Lee, J.J., Raja, D.S., and Lin, C.H. (2013). A mesoporous aluminium metal–organic framework with 3 nm open pores. J. Mater. Chem. A *1*, 324–329.

43. Wang, K., Feng, D., Liu, T.F., Su, J., Yuan, S., Chen, Y.P., Bosch, M., Zou, X., and Zhou, H.C. (2014). A series of highly stable mesoporous metalloporphyrin Fe-MOFs. J. Am. Chem. Soc. *136*, 13983–13986.

44. Li, P., Klet, R.C., Moon, S.Y., Wang, T.C., Deria, P., Peters, A.W., Klahr, B.M., Park, H.J., Al-Juaid, S.S., Hupp, J.T., and Farha, O.K. (2015). Synthesis of nanocrystals of Zr-based metal–organic frameworks with csq-net: significant enhancement in the degradation of a nerve agent simulant. Chem. Commun. *51*, 10925–10928.

45. Fujii, R., Utsunomiya, Y., Hiratake, J., Sogabe, A., and Sakata, K. (2003). Highly sensitive active-site titration of lipase in microscale culture media using fluorescent organophosphorus ester. Biochim. Biophys. Acta *1631*, 197–205.

46. Deria, P., Bury, W., Hupp, J.T., and Farha, O.K. (2014). Versatile functionalization of the NU-1000 platform by solvent-assisted ligand incorporation. Chem. Commun. *50*, 1965–1968.

47. Peters, A.W., Li, Z., Farha, O.K., and Hupp, J.T. (2015). Atomically precise growth of catalytically active cobalt sulfide on flat surfaces and within a metal–organic framework via atomic layer deposition. ACS Nano *9*, 8484–8490.

48. Modica, J.A., Skarpathiotis, S., and Mrksich, M. (2012). Modular assembly of protein building blocks to create precisely defined megamolecules. Chembiochem *13*, 2331–2334.

49. Han, S., Hermans, T.M., Fuller, P.E., Wei, Y., and Grzybowski, B.A. (2012). Transport into metal–organic frameworks from solution is not purely diffusive. Angew. Chem. Int. Ed. Engl. *51*, 2662–2666.

50. Schneider, C.A., Rasband, W.S., and Eliceiri, K.W. (2012). NIH Image to ImageJ: 25 years of image analysis. Nat. Methods *9*, 671–675.